JACS
JOURNAL OF THE AMERICAN CHEMICAL SOCIETY
Communication
pubs.acs.org/JACS

Crystal Structure of Barrel-Shaped Chiral $Au_{130}(p\text{-MBT})_{50}$ Nanocluster

Yuxiang Chen,[†] Chenjie Zeng,[†] Chong Liu,[‡] Kristin Kirschbaum,[§] Chakicherla Gayathri,[†] Roberto R. Gil,[†] Nathaniel L. Rosi,[‡] and Rongchao Jin*[,†]

[†]Department of Chemistry, Carnegie Mellon University, Pittsburgh, Pennsylvania 15213, United States
[‡]Department of Chemistry, University of Pittsburgh, Pittsburgh, Pennsylvania 15213, United States
[§]College of Natural Sciences & Mathematics, University of Toledo, Toledo, Ohio 43606, United States

Supporting Information

ABSTRACT: We report the structure determination of a large gold nanocluster formulated as $Au_{130}(p\text{-MBT})_{50}$, where *p*-MBT is 4-methylbenzenethiolate. The nanocluster is constructed in a four-shell manner, with 55 gold atoms assembled into a two-shell Ino decahedron. The surface is protected exclusively by −S−Au−S− staple motifs, which self-organize into five ripple-like stripes on the surface of the barrel-shaped Au_{105} kernel. The $Au_{130}(p\text{-MBT})_{50}$ can be viewed as an elongated version of the $Au_{102}(SR)_{44}$. Comparison of the $Au_{130}(p\text{-MBT})_{50}$ structure with the recently discovered icosahedral $Au_{133}(p\text{-TBBT})_{52}$ nanocluster (where *p*-TBBT = 4-*tert*-butylbenzenethiolate) reveals an interesting phenomenon that a subtle ligand effect in the para-position of benzenethiolate can significantly affect the gold atom packing structure, i.e. from the 5-fold twinned Au_{55} decahedron to 20-fold twinned Au_{55} icosahedron.

Solving the atomic structures of nanoparticles is of paramount importance for understanding many major issues such as the stability,[1,2] surface structure,[3−5] nucleation and growth mechanisms,[6−10] and their optical and catalytic properties.[11−14] Although significant advances have been made in solving the structures of small metal nanoclusters (i.e., with dozens of metal atoms),[15] it is still a daunting task to solve the large structures of nanoclusters with >100 metal atoms. The lack of structure information on large nanoclusters significantly hinders the fundamental understanding of the size-dependent properties and development of applications. A recent breakthrough is the successful crystallization of the $Au_{133}(p\text{-TBBT})_{52}$ nanocluster (where, *p*-TBBT = 4-*tert*-butylbenzenethiolate) with a 1.7 nm diameter metal core and 3.4 nm overall size.[16] This attainment not only demonstrates the feasibility of structure determination of nanoclusters larger than $Au_{102}(p\text{-MBA})_{44}$ (where, *p*-MBA = SPh-*p*-COOH)[17] by X-ray crystallography but also reveals the patterning strategies in fabricating giant and robust nanoclusters.[16]

In recent research, it has been found that the thiolate ligands play an important role in determining the size and structure of gold nanoclusters. Two effects of the thiolate ligand have been discovered. The first effect pertains to the steric hindrance at the α-carbon (i.e., directly connected to the sulfur in the thiolate), as demonstrated by the transformation of icosahedron-based $Au_{38}(SC_2H_4Ph)_{24}$ to cuboctahedron-based $Au_{36}(p\text{-TBBT})_{24}$.[18,19] The α-carbon hindrance effect has also been demonstrated in other systems,[20,21] and it has become a useful strategy for the discovery of new sizes and structures of gold nanoclusters.[22−25] Very recently, we have identified a second ligand effect, which is demonstrated in the case of isomeric methylbenzenethiolates (i.e., *o*-, *m*-, and *p*-MBT).[26] We found that by varying the position of the methyl group on the benzenethiolate, the most stable sizes of gold nanoclusters could be tuned from Au_{40} to Au_{104} to Au_{130} for *o*-, *m*-, and *p*-MBT, respectively.[26] This demonstrates that the subtle change of the ligand's structure can induce drastic alternation in nanocluster size. But a more detailed understanding of such a ligand effect is still missing due to the lack of structure information on this system. Herein, we report another unexpected ligand effect, which pertains to the bulkiness of the para-group (i.e., $-CH_3$ vs $-C(CH_3)_3$) on benzenethiolate. Specifically, we have successfully obtained the crystal structure of an $Au_{130}(p\text{-MBT})_{50}$ nanocluster. This nanocluster is in striking contrast with the similar-size $Au_{133}(p\text{-TBBT})_{52}$ structure, as their major structural difference is primarily dictated by the small difference in the para-group on the benzenethiolate.

The Au_{130} nanocluster was previously discovered.[27−29] Tang et al. reported the synthesis of the Au_{130} nanocluster with a mixed ligand shell, formulated as $Au_{130}(dithioldurene)_{29}(SC_2H_4Ph)_{22}$.[27] Negishi et al. used high-performance liquid chromatography to isolate an 26.3k Dalton species from a mixture of nanoclusters and determined its composition to be $Au_{130}(SC_{12}H_{25})_{50}$ by electrospray ionization mass spectrometry.[28] Jupally et al. reported a similar synthetic procedure for $Au_{130}(SC_2H_4Ph)_{50}$ through solvent fractionation and size exclusion chromatography.[29] Recently, we found that, using *p*-methylbenzenethiolate, $Au_{130}(SR)_{50}$ can be exclusively synthesized in high purity.[26] The facile synthesis of $Au_{130}(p\text{-MBT})_{50}$ and the introduction of a rigid aromatic ligand shell make it possible to crystallize this large nanocluster.

Briefly, the $Au_{130}(p\text{-MBT})_{50}$ nanocluster was synthesized by a two-step size focusing method (see Supporting Information for details).[26] In the first step, a mixture of $Au_x(p\text{-MBT})_y$ nanoclusters was synthesized by reducing $Au^I(p\text{-MBT})$ complexes with $NaBH_4$. In the second step, the size-mixed $Au_x(p\text{-MBT})_y$ nanoclusters were treated with excess of *p*-MBT thiol at 80 °C in order to select the most stable nanocluster, i.e. $Au_{130}(p\text{-MBT})_{50}$. Single crystals of $Au_{130}(p\text{-MBT})_{50}$ were obtained by

Received: May 24, 2015
Published: August 5, 2015

DOI: 10.1021/jacs.5b05378
J. Am. Chem. Soc. 2015, 137, 10076−10079

vapor diffusion of acetonitrile into a toluene solution of the nanoclusters. The structure of $Au_{130}(p\text{-MBT})_{50}$ was solved by X-ray crystallography.

The $Au_{130}(p\text{-MBT})_{50}$ can be dissected in a shell-by-shell manner, with a total of four shells. It starts with a 13-gold-atom Ino decahedron[30] (Figure 1A, upper: top view, lower: side view).

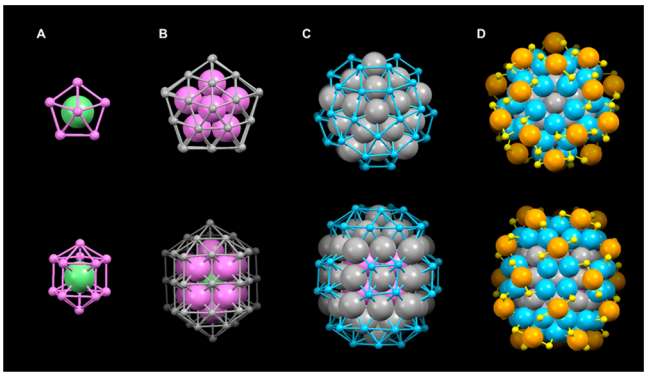

Figure 1. Four shells in the $Au_{130}(p\text{-MBT})_{50}$ nanocluster. Upper: top view; lower: side view. (A) central atom Au_1 (green) and the 1st shell Au_{12} (magenta); (B) the 2nd shell Au_{42} (gray); (C) the 3rd shell Au_{50} (blue); (D) the 4th shell Au_{25} (orange) and S_{50} (yellow).

The Au_{13} kernel is wrapped by a second shell containing 42 gold atoms, forming a two-shelled Au_{55} Ino decahedron (Figure 1B), which is indeed an isomer of the Au_{55} icosahedron discovered in the $Au_{133}(p\text{-TBBT})_{52}$ nanocluster.[16] This Au_{55} Ino decahedron is enclosed by five (111) facets at the top and another five at the bottom, as well as five (100) facets on the waist. The third shell contains 50 gold atoms and is a transition layer between the inner Au_{55} decahedron and the exterior gold−thiolate surface (Figure 1C). This layer is constructed in the following way: each of the ten (111) facets of the Au_{55} decahedron is capped with a Au_3 triangle in a hexagonal close-packed (hcp) manner, and each of the five (100) facets is capped with a Au_4 square, thus $10 \times 3 + 5 \times 4 = 50$ atoms. The three-shelled Au_{105} kernel exhibits quasi-D_{5h} symmetry, resembling a pentagonal barrel (Figure 1C).

The fourth shell contains 25 gold atoms and 50 sulfur atoms, which assemble into 25 monomeric −S−Au−S− staple motifs. These 25 staple motifs provide full protection to the exposed 50 surface gold atoms in the third shell (Figure 1C, blue), with each staple motif stabilizing two gold atoms by S−Au bonds (Figure 1D). The position of each −S−Au−S− motif is on the diagonal of an Au_4 square or rectangle (Figure 1D, blue), since the span of two sulfur atoms in −S−Au−S− matches with the distance of two diagonal Au atoms in the square or rectangle.

The −S−Au−S− staple motifs self-organize into "ripple-like" stripe patterns on the surface of the Au_{105} kernel (Figure 2). Five staple motifs are aligned in a circle, forming a pentagonal ripple (Figure 2A). There are five such pentagonal ripples on different latitudes of the Au_{105} kernel (Figure 2B, C). The ripples have different radii, with the one at the equator of the Au_{105} kernel being the largest, and the two at the top/bottom poles being the smallest, accommodating the barrel shape of the interior Au_{105} kernel. The overall $Au_{130}S_{50}$ framework maintains the barrel (diameter: 1.6 nm, height: 1.9 nm), and the five −S−Au−S− ripple stripes resemble the metal hoops that bind the wooden staves into a barrel shape (Figure 2C, brown shadow). The $Au_{130}S_{50}$ framework exhibits quasi-D_5 symmetry, with one C_5 axis passing through the top/bottom poles and five C_2 axes at the equator. This structure is chiral due to the different rotative

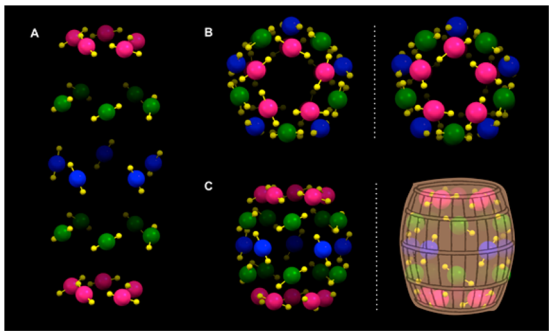

Figure 2. Chiral surface patterns of −S−Au−S− pentagon ripples on the Au_{105} kernel. (A) Five pentagon ripples; (B) top view; (C) side view. Red/Green/Blue: gold. Yellow: sulfur.

arrangement of the −S−Au−S− motifs (Figure 2B, C). The left- and right-handed enantiomers are found in the unit cell of the $Au_{130}(p\text{-MBT})_{50}$ crystal. The harmony of the 5-fold symmetry in the $Au_{130}(p\text{-MBT})_{50}$ is responsible for its high stability.

The carbon atoms cannot be fully resolved in the X-ray crystallography analyses of the $Au_{130}(p\text{-MBT})_{50}$ nanocluster. In order to probe the packing structure of the carbon groups, we employed 1D and 2D nuclear magnetic resonance (NMR) (see Supporting Figures S1−S3).[31] As shown in Figure S1A, the HS−C_6H_4−p-CH_3 thiol shows proton chemical shifts at 2.30 (corresponding to −p-CH_3, denoted as γ-H) and 7.26/7.21, 7.07/7.04 ppm (corresponding to −C_6H_4−, denoted as α-H and β-H). When the thiolates are assembled on the surface of $Au_{130}(p\text{-MBT})_{50}$, the chemical shifts of H atoms are split into multiple sets of peaks, ranging from 8.2 to 6.0 ppm (in aromatic region) and 2.5 to 1.9 ppm (in methyl region); see Figure S1B. The splittings reflect that the thiolates are in different chemical environments. Analysis of the sets of peaks and their intensities provides information on the symmetry in the assembly of carbon tails.[31] Using a 2D correlation spectrum (^{1}H−^{1}H COSY), the α-, β-, and γ-H signals from the same thiolate can be correlated (Figure 3). We found that the 50 p-MBTs are split into 5 groups,

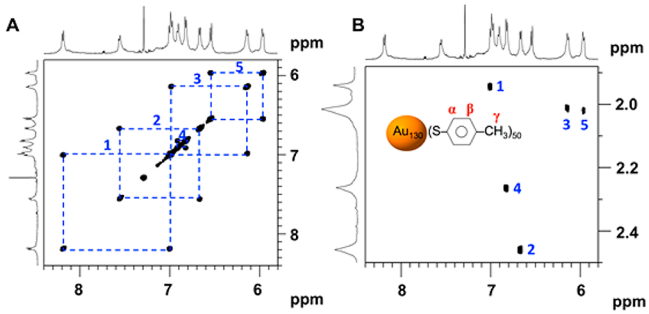

Figure 3. Two-dimensional NMR of $Au_{130}(p\text{-MBT})_{50}$. (A) ^{1}H−^{1}H COSY of α-H and β-H; (B) ^{1}H−^{1}H COSY of β-H and γ-H.

with each group containing 10 identical p-MBTs (Figure 3). The detailed chemical shifts of each set of peaks and their integrations are provided in the Supporting Figures S1−S3 and Table S1.

This 5-fold splitting pattern of carbon groups indeed correlates with the D_5 symmetry of the surface structure in the $Au_{130}S_{50}$ framework. In the fourth $Au_{25}S_{50}$ shell, the sulfur atoms are arranged into 10 layers from the top to the bottom (corresponding to 5 −S−Au−S− layers, Figure 2C). Due to the C_2 axes at the equator, the 1st and 10th layers of sulfur atoms are of the same chemical environment, and likewise the second

DOI: 10.1021/jacs.5b05378
J. Am. Chem. Soc. 2015, 137, 10076−10079

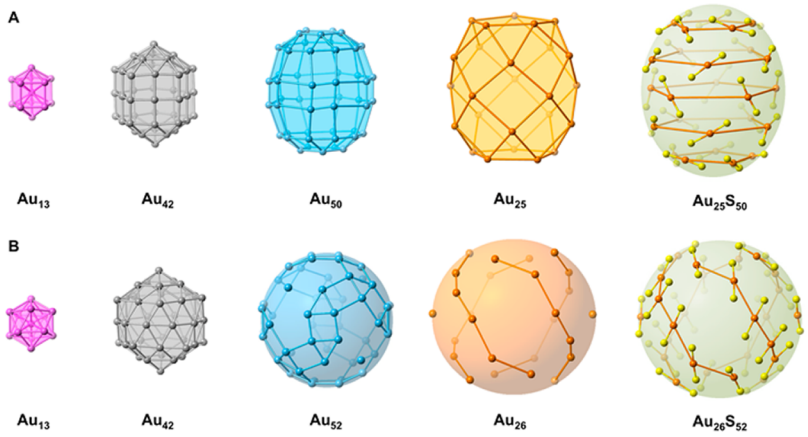

Figure 4. Comparison of the $Au_{130}(p\text{-MBT})_{50}$ structure (A) with the $Au_{133}(p\text{-TBBT})_{52}$ structure (B) in a shell-by-shell manner.

and ninth, third and eighth, etc. Thus, there are five groups of sulfur atoms in distinct environments, with each group containing 10 sulfur atoms. The 5 groups of carbon tails determined by 2D-NMR are consistent with the 5 sets of inequivalent sulfur atoms as determined by the X-ray structure, which indicates that each group of carbon tails is attributed to each layer of sulfur atoms, and the carbon tails are arranged in a similar layered fashion. The further correlation between the five sets of NMR signals and the five domains in the structure of $Au_{130}(p\text{-MBT})_{50}$ however requires theoretical calculations of the local electron densities.

It is worth noting that a similar structure model of $Au_{130}(SR)_{50}$ was proposed by Negishi et al.[28] It was predicted to be composed of a Au_{75} Marks decahedron capped by two Au_{15} motifs, which is further protected by 25 monomeric staple motifs. Note that the Au_{75} Marks decahedron is evolved from the Au_{55} Ino decahedron by capping its five (100) facets with 20 more gold atoms.[32] The structure of $Au_{130}(SR)_{50}$ was deduced from the $Au_{102}(SR)_{44}$, which contains a Au_{49} Marks decahedron (one layer of atoms less than Au_{75}) capped by the same Au_{15} motifs.[17] The same structure model was also proposed by Tlahuice-Flores et al. based on scanning transmission electron microscopy (STEM) imaging and density functional theory (DFT) calculation of $Au_{130}(SR)_{50}$.[33] There is actually a close relationship between the $Au_{130}(SR)_{50}$ and the $Au_{102}(SR)_{44}$ (Figure S4); that is, both nanoclusters can be included in the family of decahedra, and the $Au_{130}(SR)_{50}$ can be viewed as an elongated version of the $Au_{102}(SR)_{44}$. It is this elongation that creates an additional layer of "foot-holds" in the third shell (Figure 1C, blue), which makes it possible to form ordered surface patterns of −S−Au−S− ripple stripes in $Au_{130}(SR)_{50}$. In the $Au_{102}(SR)_{44}$, there is only partial ordering of the −S−Au−S− staples at the poles, while the distribution of gold−thiolate motifs is random at the waist[34] (Figure S4).

The $Au_{130}(p\text{-MBT})_{50}$ has a close formula with the recently discovered $Au_{133}(p\text{-TBBT})_{52}$,[16] and these two structures share some structural construction rules. For example, both nanoclusters are constructed in a shell-by-shell manner with a total of four shells (Figure 4). Also, their surfaces are protected exclusively by the −S−Au−S− monomer motifs. The −S−Au−S− motifs tend to adopt parallel alignment and further self-organize into large-scale surface patterns (Figures 2 and 4, right).

On the other hand, the two structures exhibit some interesting differences. First of all, the structure of $Au_{130}(p\text{-MBT})_{50}$ is based on a Au_{55} Ino decahedron, whereas the $Au_{133}(p\text{-TBBT})_{52}$ is based on a Au_{55} icosahedron (Figure 4). The major difference between the two Au_{55} polyhedra is at the middle three layers, which are eclipsed in the decahedron but are staggered in the icosahedron (Figure 4, gray). The eclipsed pentagon layers make the Au_{55} decahedron a 5-fold twinned structure, with a slightly anisotropic shape, i.e. 12 Å in height vs 10 Å in diameter. The anisotropy of the decahedron is further amplified in the third and fourth shells, making the final Au_{130} a barrel shape (Figure 4A). In contrast, the Au_{55} icosahedron in $Au_{133}(p\text{-TBBT})_{52}$ is a 20-fold twinned structure with a nearly perfect isotropic shape with a radius of 5.6 Å, and the spherical shape is maintained during the growth of the third and fourth shells (Figure 4B).

Second, the −S−Au−S− motifs form different surface patterns in the two nanoclusters. In $Au_{130}(p\text{-MBT})_{50}$, the −S−Au−S− motifs form *ripple*-like stripes, circling around the C_5 axis at different latitudes of the inner barrel (Figure 4A, right), while in $Au_{133}(p\text{-TBBT})_{52}$, the −S−Au−S− motifs assemble into *helical* stripes, wrapping along the *longitudes* of the inner sphere (Figure 4B, right). These two structures demonstrate the surface-ordering strategies in constructing large $Au_n(SR)_m$ nanoclusters and also reflect that different surface patterns would be formed in accordance to the different curvature of the kernel and hindrance of the thiolates.

It is known that bare metal clusters in the gas phase differ in energy between the icosahedral and decahedral atomic arrangements.[35] It was predicted that the icosahedron is more favorable in smaller sizes than the decahedron due to the icosahedron's lower *surface energy* (i.e., the smaller surface-to-volume ratio, and also being exclusively enclosed by close-pack (111) facets).[35] But in larger sizes, the decahedron becomes preferred due to its lower *volume energy* (i.e., less internal strain of 5-fold twinning in decahedra than 20-fold twinning in icosahedra). Interestingly, in ligand-protected gold nanoclusters, the two polyhedra of similar size appear to be selected by different surface-protecting ligands. This indicates that the surface stress introduced by the interaction of thiolates in the ligand shell considerably contributes to the total energy of the nanocluster.

The different structures in $Au_{130}(p\text{-MBT})_{50}$ and $Au_{133}(p\text{-TBBT})_{52}$ demonstrate that the structure of $Au_n(SR)_m$ nanoclusters is quite sensitive to the subtle change of thiolate ligand structure, especially in large nanoclusters. This effect of the substituent in the para-position is unexpected: we originally thought that the *p*-MBT would be equivalent to *p*-TBBT, because the difference is merely at the end of the thiolate ($-CH_3$ vs $-C(CH_3)_3$), which is far away from the sulfur head and would

DOI: 10.1021/jacs.5b05378
J. Am. Chem. Soc. 2015, 137, 10076−10079

less affect the S−Au bonding; the latter was indeed true for smaller-sized $Au_{36}(SR)_{24}$ nanoclusters (i.e., Au_{36} can be synthesized by both the *p*-MBT and *p*-TBBT). But the difference is amplified in larger sizes of nanoclusters, and different sizes are selected by *p*-MBT and *p*-TBBT, respectively.

For a stabilized surface, there exists a balance between attraction and repulsion: on one hand, ligands should not be too close, in order to avoid the stress in the ligand shell; on the other hand, the ligands should not be too separated, which would reduce the attraction between the ligands (e.g., $\pi-\pi$ stacking) and also result in vacancies in the ligand shell, hence, possible attacks by other molecules. Packing the molecules on the 3D curved surface is a more complicated case than the 2D flat surface. The packing efficiency is not only determined by the ligand structure, surface area, but also influenced by the surface curvature. Figure S5 compares the *p*-MBT and *p*-TBBT, with a major difference in the bulkiness of the para-group. The methyl group has a projected radius of 0.9 Å, like a small dot attached to the benzene ring, while the *tert*-butyl group has a much larger projected radius of 2.1 Å, resembling an umbrella. If both thiolates adopt the parallel packing on the flat surface, the space between *p*-MBT would be less than the *p*-TBBT (Figure S5B). In contrast, if the ligands are assembled on the curved surface, the *p*-TBBT would require more surface curvature than MBT (Figure S5C) to avoid the steric hindrance of the *tert*-butyl group. This can partially explain why *p*-TBBT gives rise to a spherical shape in Au_{133} while *p*-MBT to a barrel shape in Au_{130}. In the similar sized sphere and barrel, the sphere has a larger surface curvature. The total surface area of the Au_{130} barrel is calculated to be 792 $Å^2$, with 15.9 $Å^2$ per ligand; for the Au_{133} sphere, the surface area is 907 $Å^2$, with 17.4 $Å^2$ per ligand. It is worth noting that the surface curvature effect is amplified in larger sizes, because the larger sizes have generally smaller surface curvature, and it is more sensitive to subtle changes of ligands' packing structures. A more quantitative study of the para-group effect in the size and structure of nanoclusters calls for theoretical calculations.[36]

■ ASSOCIATED CONTENT

Supporting Information

The Supporting Information is available free of charge on the ACS Publications website at DOI: 10.1021/jacs.5b05378.

Details of the synthesis, crystallization, X-ray analysis, NMR, and supporting Figures S1−S5 and Tables S1−S6 (PDF)

Crystallographic data (CIF)

■ AUTHOR INFORMATION

Corresponding Author

*rongchao@andrew.cmu.edu

Notes

The authors declare no competing financial interest.

■ ACKNOWLEDGMENTS

The work is supported by the Air Force Office of Scientific Research under AFOSR Award No. FA9550-15-1-9999 (FA9550-15-1-0154), the NSF MRI NMR instrumentation award CHE-1039870 and the Camille Dreyfus Teacher-Scholar Awards Program. We thank Dr. Huifeng Qian for discussion on NMR analysis and Kelly J. Lambright for assistance with the crystallography.

■ REFERENCES

(1) Qian, H.; Zhu, M.; Wu, Z.; Jin, R. *Acc. Chem. Res.* **2012**, *45*, 1470.
(2) Maity, P.; Xie, S.; Yamauchi, M.; Tsukuda, T. *Nanoscale* **2012**, *4*, 4027.
(3) Zeng, C.; Liu, C.; Chen, Y.; Rosi, N. L.; Jin, R. *J. Am. Chem. Soc.* **2014**, *136*, 11922.
(4) Wan, X. K.; Yuan, S. F.; Tang, Q.; Jiang, D. E.; Wang, Q. M. *Angew. Chem., Int. Ed.* **2015**, *54*, 5977.
(5) Wang, Y.; Su, H.; Xu, C.; Li, G.; Gell, L.; Lin, S.; Tang, Z.; Hakkinen, H.; Zheng, N. *J. Am. Chem. Soc.* **2015**, *137*, 4324.
(6) Zeng, C.; Chen, Y.; Li, G.; Jin, R. *Chem. Commun.* **2014**, *50*, 55.
(7) Pei, Y.; Zeng, X. C. *Nanoscale* **2012**, *4*, 4054.
(8) Jiang, D.-e.; Overbury, S. H.; Dai, S. *J. Am. Chem. Soc.* **2013**, *135*, 8786.
(9) Shichibu, Y.; Zhang, M.; Kamei, Y.; Konishi, K. *J. Am. Chem. Soc.* **2014**, *136*, 12892.
(10) Yu, Y.; Nachammai, V.; Zhang, B.; Yan, N.; Leong, D. T.; Jiang, D.-e.; Xie, J.; Luo, Z. *J. Am. Chem. Soc.* **2014**, *136*, 10577.
(11) Yu, Y.; Luo, Z.; Chevrier, D. M.; Leong, D. T.; Zhang, P.; Jiang, D.-e.; Xie, J. *J. Am. Chem. Soc.* **2014**, *136*, 1246.
(12) Yamazoe, S.; Koyasu, K.; Tsukuda, T. *Acc. Chem. Res.* **2014**, *47*, 816.
(13) Li, H.; Li, L.; Pedersen, A.; Gao, Y.; Khetrapal, N.; Jónsson, H.; Zeng, X. C. *Nano Lett.* **2015**, *15*, 682.
(14) Kawasaki, H.; Kumar, S.; Li, G.; Zeng, C.; Kauffman, D. R.; Yoshimoto, J.; Iwasaki, Y.; Jin, R. *Chem. Mater.* **2014**, *26*, 2777.
(15) Jin, R. *Nanoscale* **2015**, *7*, 1549.
(16) Zeng, C.; Chen, Y.; Kirschbaum, K.; Appavoo, K.; Sfeir, M. Y.; Jin, R. *Sci. Adv.* **2015**, *1*, e1500045.
(17) Jadzinsky, P. D.; Calero, G.; Ackerson, C. J.; Bushnell, D. A.; Kornberg, R. D. *Science* **2007**, *318*, 430.
(18) Zeng, C.; Qian, H.; Li, T.; Li, G.; Rosi, N. L.; Yoon, B.; Barnett, R. N.; Whetten, R. L.; Landman, U.; Jin, R. *Angew. Chem., Int. Ed.* **2012**, *51*, 13114.
(19) Zeng, C.; Liu, C.; Pei, Y.; Jin, R. *ACS Nano* **2013**, *7*, 6138.
(20) Nishigaki, J. I.; Tsunoyama, R.; Tsunoyama, H.; Ichikuni, N.; Yamazoe, S.; Negishi, Y.; Ito, M.; Matsuo, T.; Tamao, K.; Tsukuda, T. *J. Am. Chem. Soc.* **2012**, *134*, 14295.
(21) Krommenhoek, P. J.; Wang, J.; Hentz, N.; Johnston-Peck, A. C.; Kozek, K. A.; Kalyuzhny, G.; Tracy, J. B. *ACS Nano* **2012**, *6*, 4903.
(22) Das, A.; Li, T.; Nobusada, K.; Zeng, C.; Rosi, N. L.; Jin, R. *J. Am. Chem. Soc.* **2013**, *135*, 18264.
(23) Crasto, D.; Malola, S.; Brosofsky, G.; Dass, A.; Häkkinen, H. *J. Am. Chem. Soc.* **2014**, *136*, 5000.
(24) Song, Y.; Wang, S.; Zhang, J.; Kang, X.; Chen, S.; Li, P.; Sheng, H.; Zhu, M. *J. Am. Chem. Soc.* **2014**, *136*, 2963.
(25) Zeng, C.; Chen, Y.; Li, G.; Jin, R. *Chem. Mater.* **2014**, *26*, 2635.
(26) Chen, Y.; Zeng, C.; Kauffman, D. R.; Jin, R. *Nano Lett.* **2015**, *15*, 3603.
(27) Tang, Z.; Robinson, D. A.; Bokossa, N.; Xu, B.; Wang, S.; Wang, G. *J. Am. Chem. Soc.* **2011**, *133*, 16037.
(28) Negishi, Y.; Sakamoto, C.; Ohyama, T.; Tsukuda, T. *J. Phys. Chem. Lett.* **2012**, *3*, 1624.
(29) Jupally, V. R.; Dass, A. *Phys. Chem. Chem. Phys.* **2014**, *16*, 10473.
(30) Ino, S. *J. Phys. Soc. Jpn.* **1969**, *27*, 941.
(31) Qian, H.; Zhu, M.; Gayathri, C.; Gil, R. R.; Jin, R. *ACS Nano* **2011**, *5*, 8935.
(32) Marks, L. *Philos. Mag. A* **1984**, *49*, 81.
(33) Tlahuice-Flores, A.; Santiago, U.; Bahena, D.; Vinogradova, E.; Conroy, C. V.; Ahuja, T.; Bach, S. B. H.; Ponce, A.; Wang, G.; José-Yacamán, M.; Whetten, R. L. *J. Phys. Chem. A* **2013**, *117*, 10470.
(34) Mednikov, E. G.; Dahl, L. F. *Small* **2008**, *4*, 534.
(35) Baletto, F.; Ferrando, R. *Rev. Mod. Phys.* **2005**, *77*, 371.
(36) Tang, Q.; Ouyang, R.; Tian, Z.; Jiang, D.-e. *Nanoscale* **2015**, *7*, 2225.

DOI: 10.1021/jacs.5b05378
J. Am. Chem. Soc. 2015, 137, 10076−10079